UV light activates a $G\alpha_{q/11}$-coupled phototransduction pathway in human melanocytes

Nicholas W. Bellono,[1] Julia A. Najera,[2] and Elena Oancea[1]

[1]Department of Molecular Pharmacology, Physiology, and Biotechnology, and [2]Department of Neuroscience, Brown University, Providence, RI 02192

While short exposure to solar ultraviolet radiation (UVR) can elicit increased skin pigmentation, a protective response mediated by epidermal melanocytes, chronic exposure can lead to skin cancer and photoaging. However, the molecular mechanisms that allow human skin to detect and respond to UVR remain incompletely understood. UVR stimulates a retinal-dependent signaling cascade in human melanocytes that requires GTP hydrolysis and phospholipase C β (PLCβ) activity. This pathway involves the activation of transient receptor potential A1 (TRPA1) ion channels, an increase in intracellular Ca^{2+}, and an increase in cellular melanin content. Here, we investigated the identity of the G protein and downstream elements of the signaling cascade and found that UVR phototransduction is $G\alpha_{q/11}$ dependent. Activation of $G\alpha_{q/11}$/PLCβ signaling leads to hydrolysis of phosphatidylinositol (4,5)-bisphosphate (PIP_2) to generate diacylglycerol (DAG) and inositol 1, 4, 5-trisphosphate (IP_3). We found that PIP_2 regulated TRPA1-mediated photocurrents, and IP_3 stimulated intracellular Ca^{2+} release. The UVR-elicited Ca^{2+} response appears to involve both IP_3-mediated release from intracellular stores and Ca^{2+} influx through TRPA1 channels, showing the fast rising phase of the former and the slow decay of the latter. We propose that melanocytes use a UVR phototransduction mechanism that involves the activation of a $G\alpha_{q/11}$-dependent phosphoinositide cascade, and resembles light phototransduction cascades of the eye.

The Journal of General Physiology

INTRODUCTION

Sunlight is crucial for life and has many beneficial effects, but, at the same time, the UV radiation (UVR) contained by sunlight is the most common environmental carcinogen (Routaboul et al., 1999; Bennett, 2008). Unlike other mammals that have fur to protect their skin, human skin is constantly exposed to solar UVR (280–400 nm) and is susceptible to its damaging effects, primarily skin cancers and photoaging. Human skin also has a unique protection mechanism against UVR: the presence of melanocytes in the epidermis allows skin to respond to UVR by increasing its pigmentation. Because UVR is omnipresent and is able to interact with human skin, identifying the molecular pathways that allow human skin to detect and elicit an immediate response to UVR is critical for developing new photoprotective methods.

How does human skin detect UVR? UVR consists of photons; photons can activate G protein–coupled opsin receptors (GPCRs) in the eye that elicit cellular responses through the activation of different G proteins and downstream effectors. $G\alpha_{i/o}$ is used by vertebrate photoreceptors (Fung et al., 1981), whereas $G\alpha_{q/11}$ mediates *Drosophila melanogaster* phototransduction (Hardie, 2001) and non-image forming vision in the mammalian retina (Berson et al., 2002; Panda et al., 2005; Yau and Hardie, 2009). Activation of $G\alpha_{q/11}$ pathways leads to stimulation of phospholipase C β (PLCβ), which induces hydrolysis of phosphatidylinositol 4,5-bisphosphate (PIP_2) into diacylglycerol (DAG) and inositol 1,4,5-trisphosphate (IP_3). Changes in the levels of PIP_2, DAG, and IP_3 modulate the activity of many proteins, including transient receptor potential (TRP) ion channels.

We recently characterized a retinal-dependent UVR-sensitive phototransduction pathway in human epidermal melanocytes (HEMs) that is G protein and PLCβ dependent and results in the activation of TRP subfamily A1 (TRPA1) channels; activation of this pathway results in a rapid increase in intracellular Ca^{2+} ($[Ca^{2+}]_{ic}$) and increased cellular melanin content (Wicks et al., 2011; Bellono et al., 2013). In this study we investigated the G protein that mediates this pathway and the downstream molecular events. We found that UVR phototransduction in HEMs is mediated by $G\alpha_{q/11}$ signaling, and provide evidence for a phosphoinositide cascade

N.W. Bellono and J.A. Najera contributed equally to this paper.
Correspondence to Elena Oancea: elena_oancea@brown.edu

Abbreviations used in this paper: CA, cinnamaldehyde; CTX, cholera toxin; DAG, diacylglycerol; GPCR, G protein–coupled opsin receptor; HEM, human epidermal melanocyte; IP_3, inositol 1,4,5-trisphosphate; IP_3R, IP_3 receptor; miRNA, microRNA; OAG, 1-oleoyl-2-acetyl-*sn*-glycerol; PC-PLC, phosphatidylcholine phospholipase C; PH, pleckstrin homology; PIP_2, phosphatidylinositol 4,5-bisphosphate; PIP_3, $PI(3,4,5)P_3$; PLCβ, phospholipase C β; qPCR, quantitative PCR; PTX, pertussis toxin; RGS, regulators of G protein signaling; TRP, transient receptor potential; UVR, UV radiation; XeC, Xestospongin C.

The Rockefeller University Press $30.00
J. Gen. Physiol. Vol. 143 No. 2 203–214
www.jgp.org/cgi/doi/10.1085/jgp.201311094

involving IP_3-mediated intracellular Ca^{2+} release via IP_3 receptors (IP_3R) and PIP_2 regulation of Ca^{2+}-permeable TRPA1 ion channels. The two sources of Ca^{2+} have different dynamics and, combined, result in a Ca^{2+} response with a fast rising phase and a slow decay. Our results demonstrate that UVR phototransduction in HEMs activates a $G\alpha_{q/11}$-dependent signaling pathway similar to well-characterized phototransduction pathways in the eye.

MATERIALS AND METHODS

Reagents

Cholera toxin (CTX), pertussis toxin (PTX), HC-030031, 1-oleoyl-2-acetyl-*sn*-glycerol (OAG), phosphatidylcholine phospholipase C (PC-PLC; from *Clostridia perfringens*), polylysine (PolyK, 70–150 kD), heparin, and ionomycin were purchased from Sigma-Aldrich. Endothelin, GPAnt-2, GPAnt-2a, and Xestospongin C (XeC) were from Tocris Bioscience. mSIRK and L9A were from EMD Millipore. DiC8-PIP2 was from Echelon Biosciences. Stocks of all reagents in water, DMSO, or ethanol were stored at −4°C or −20°C until use and diluted to the final concentration to contain <1% solvent. For Ca^{2+} imaging experiments, HEMs were preincubated with pharmacological reagents for 3–15 min, with the exception of PTX and CTX, which used 24 h incubations.

Cell culture

Primary HEMs isolated from neonatal foreskin were cultured in Medium 254 containing Human Melanocyte Growth Supplement (HMGS2; Cascade Biologics/Invitrogen) and 1% penicillin-streptomycin (Invitrogen), and propagated for a limited number of cell divisions (≤15). Vitamin A or retinoid derivatives are not components of either Medium 254 or HMGS2. Human embryonic kidney (HEK293) cells were cultured in Dulbecco's Modified Eagle Medium and F12 nutrient mixture (DMEM-F12; Gibco/Invitrogen) containing 10% fetal bovine serum (Atlanta Biologicals) and 1% penicillin-streptomycin (Invitrogen).

Molecular biology

MicroRNAs (miRNAs) were designed and expressed in HEMs using a lentiviral system, as described previously (Wicks et al., 2011). BLOCK-iT miRNA oligos (Invitrogen) were cloned into the pcDNA6.2-GW/EmGFP-miR expression vector modified to contain mCherry instead of EmGFP to allow for simultaneous fluorescence detection and Fluo-4–based Ca^{2+} imaging. miRNAs were recombined from pcDNA6.2-GW into pDONR221 and pLENTI6/V5-DEST vectors (Invitrogen) for lentiviral production. Lentiviral particles containing miRNA were obtained as described previously (Wicks et al., 2011). HA-tagged RGS2 (Missouri S&T cDNA Resource Center) was recombined into pDONR221 and pLENTI6/V5-DEST vectors (Invitrogen) for lentiviral production as described previously (Wicks et al., 2011).

The mRNA expression level of $G\alpha_q$, $G\alpha_{11}$, or $G\alpha_{q/11}$ in control or targeted miRNA-treated cells was determined ≥7 d after infection using comparative C_T quantitative PCR (qPCR). Total RNA was extracted from infected HEMs using the RNeasy Plus kit (QIAGEN) and converted to cDNA using RT-PCR (SuperScript III; Invitrogen). qPCR reactions were prepared according to manufacturer instructions using Power SYBR green. All reactions were done in triplicate and actin was used for normalization.

Western blots

Expression of HA-tagged RGS2 in HEMs was confirmed via Western blotting. Cells were homogenized ≥10 d after infection in ice-cold RIPA buffer (Thermo Fisher Scientific) containing protease inhibitor cocktail (Roche). Samples were agitated at 4°C for 30 min and then centrifuged at 16,000 *g* for 30 min at 4°C. Protein content was determined using the Pierce BCA Protein Assay kit (Thermo Fisher Scientific). Equal amounts of protein were loaded onto each lane, separated by electrophoresis on NuPAGE Bis-Tris gels (Invitrogen), and transferred to PVDF membranes (Roche). Membranes were blocked at room temperature for 1 h and incubated overnight at 4°C with rat monoclonal anti-HA antibody clone 3F10 (1:500; Roche), followed by 1 h at room temperature with HRP-conjugated goat anti–rat IgG affinity-purified antibody (1:5,000; EMD Millipore). Antibodies were detected using the SuperSignal West Femto enhanced chemiluminescence system (Thermo Fisher Scientific) and imaged using autoradiography film (Thermo Fisher Scientific).

Light stimulation

Ultraviolet light stimulation of cultured HEMs was conducted using a 200 W Hg-Xe arc lamp with converging optics and appropriate filters (Wicks et al., 2011). A dichroic mirror (260–400 nm) was used in combination with 280-nm long pass and a 400-nm short pass filters (Newport). The levels of light lost due to scattering by imaging buffer were negligible. Physiological doses of UVR were applied by varying the duration and/or power of the pulse. A hand-held silicon detector was used to measure power (Newport).

Calcium imaging

Ca^{2+} imaging was performed as described previously (Wicks et al., 2011; Bellono et al., 2013). Cultured HEMs plated on glass coverslips were incubated for 15 min at room temperature in Ringer's solution with 2 µM Fluo-4 (Molecular Probes/Invitrogen) and 250 µM sulfinpyrazone (Sigma-Aldrich), followed by dark incubation for 15 min with 12 µM of 9-cis or all-trans retinal (Sigma-Aldrich). Imaging was performed in modified Ringer's extracellular solution containing (in mM): 150 NaCl, 1.8 $CaCl_2$, 1.2 $MgCl_2$, 10 D glucose, 25 HEPES, pH 7.4, and 310 mOsm/liter. Fluorescence images were acquired every 2 s, and 2 µM ionomycin (Sigma-Aldrich) was added at the end of some experiments to elicit a maximal Ca^{2+} response used for normalization.

The fluorescence intensity of individual cells (measured using ≥25% of the cell area, F_{cell}) was quantified using MetaMorph (Molecular Devices) and MATLAB (MathWorks) and plotted in Prism 6 (GraphPad Software). F_{cell} values were normalized as $F_{norm} = (F_{cell} - F_{min})/(F_{iono} - F_{min})$, where F_{iono} is maximal fluorescence with ionomycin, and F_{min} is baseline fluorescence averaged from ≥15 data points acquired before light stimulation. Final data values for each dish were obtained by averaging F_{norm} values from individual cells. In experiments where ionomycin was not used for normalization, Fluo-4 fluorescence intensities were quantified as $\Delta F/F_o(t) = [F_{cell}(t) - F_{baseline}]/F_{baseline}$ and averaged as described previously. $\Delta F/F_o$ values were plotted as a function of time and fitted with a single-exponential function in Prism 6 (GraphPad Software) to calculate decay time constants. Ca^{2+} response initial slopes were calculated over the first 30 s after UVR stimulation.

Paired Ca^{2+} imaging experiments were used when the dish-to-dish variability was significant. Cells for each of the paired experiments were plated on glass coverslips and treated identically by incubation in the same Fluo-4 and retinal solution, then imaged sequentially in alternating order: control followed by experimental condition or experimental condition followed by control. The averaged fluorescence intensities of cells from one coverslip measured in each condition were plotted as the two experimental values connected by the dotted line. Statistical significance of paired experiments was evaluated using a paired Student's *t* test. When pairing is not mentioned, the cells were cultured and treated identically, but we did not strictly alternate control and experimental condition measurements. In such cases, we averaged the values from all the control and all the experimental conditions and represented them as bar graphs.

Electrophysiology

Electrophysiology experiments were performed as described previously (Bellono et al., 2013). All-trans retinal was stored, solubilized, and applied as described previously (Wicks et al., 2011). Experiments were performed under dim-red or infrared illumination. Whole-cell patch clamp recordings were carried out using micropipettes with 3–6 MΩ resistance at room temperature using an EPC 10 amplifier (HEKA) with PatchMaster software (HEKA), filtered at 2.9 kHz and digitized at 20 kHz. Experiments were performed using modified Ringer's solution (see "Calcium imaging"). Unless stated otherwise, internal pipette solution contained (in mM): 140 CsCl, 1 $MgCl_2$, 4 MgATP, 10 EGTA, 10 HEPES, pH 7.2, and 290 mOsm/liter. The low EGTA solution used in Fig. S3 contained 20 µM EGTA. UVR-induced currents were measured using a step protocol consisting of a step from a holding potential of −60 mV to +80 mV immediately before UVR exposure. Current values were calculated by subtracting initial current at +80 mV (I_o) from maximal current after UVR exposure: $I_{UVR} = I_{max} - I_o$. All recordings were inspected for baseline drift before analysis. In most recordings, the baseline did not drift significantly. If the baseline drift was >20% of the UVR response, cells were excluded. Cell membrane capacitance values were used to calculate current densities. Current–voltage (I-V) relations were established using voltage step protocol from the −60-mV holding potential to voltages between −80 mV and +80 mV in 20-mV increments.

HEMs are very difficult to patch clamp. Our experiments are further complicated by the fact that UV exposure often causes us to lose patches. Because UV photocurrents are small and exhibit strong outward rectification (Bellono et al., 2013), most of our voltage-clamp experiments use positive membrane voltages that are not physiological (+80 mV) in order to increase current amplitude. Although current amplitude is higher at positive membrane voltages, current kinetics are significantly altered compared with recordings carried out at more physiological membrane voltages (Bellono and Oancea, 2013). In addition, positive voltages are not well tolerated by these cells, preventing us from recording and plotting the current over a long period of time for every single trace. We have previously recorded currents over longer periods using voltage pulses (Bellono et al., 2013) and at more negative voltages (Bellono and Oancea, 2013), and showed that the current returns to baseline after the UV pulse. Our success rate, even for the short periods of UV irradiation, is well below 10%. Consistent with the difficultly of these experiments, the large noise is likely caused by the relatively low seal resistance (∼1 GΩ) and patch stability.

Statistical analyses

Experimental data are presented as mean ± SEM, where *n* refers to the number of dishes for imaging data or the number of cells for electrophysiology. We calculated p-values by unpaired or paired Student's *t* test and considered results significant when P ≤ 0.05.

Online supplemental material

Fig. S1 shows that RGS2 expression in HEMs reduces Ca^{2+} responses to endothelin. Fig. S2 shows that HEMs expressing $G\alpha_q$-, $G\alpha_{11}$-, or $G\alpha_{q/11}$-targeted miRNA have reduced Ca^{2+} responses to endothelin. Fig. S3 shows that neither IP_3-mediated Ca^{2+} release nor DAG activate the UVR photocurrent. Fig. S4 shows selective inhibition of UVR phototransduction signaling components versus ion channels by cellular dialysis. Online supplemental material is available at http://www.jgp.org/cgi/content/full/jgp.201311094/DC1.

RESULTS

Identification of the Gα subunit that mediates UVR-induced Ca^{2+} responses in HEMs

We have recently shown that exposure to physiological doses of UVR activates a retinal-dependent phototransduction pathway that is mediated by G protein activation (Wicks et al., 2011; Bellono et al., 2013). However, we have yet to identify the type of G protein responsible for initiating the retinal-dependent signaling pathway activated by UVR. HEMs express a variety of GPCRs and their related G proteins, including the melanocortin-1 receptor coupled to $G\alpha_s$ (Park et al., 2009) and the $G\alpha_{q/11}$-coupled endothelin-1B (ET-1) receptor (Yada et al., 1991; Imokawa et al., 1992).

Because we previously showed that UVR exposure leads to retinal-dependent Ca^{2+} responses (Wicks et al., 2011), we monitored intracellular Ca^{2+} levels using the fluorometric Ca^{2+} indicator Fluo-4 in response to treatments that modulate the function of different G protein subunits. We first tested if UVR-induced Ca^{2+} responses in HEMs were mediated by members of the $G\alpha_s$ or $G\alpha_{i/o}$ family. CTX treatment inhibits $G\alpha_s$-mediated signaling and PTX inhibits $G\alpha_{i/o}$ signaling (Beckman et al., 1974; Malbon et al., 1984). HEMs incubated for 24 h with 500 ng/ml CTX, 500 ng/ml PTX, or vehicle, and stimulated with 150 mJ/cm^2 UVR showed no difference in the amplitude of retinal-dependent Ca^{2+} responses (Fig. 1, A and B; amplitude of the response: $F_{norm,\ max} = 0.55 \pm 0.04$ for vehicle, 0.56 ± 0.05 for CTX, 0.52 ± 0.04 for PTX). This result suggests that Ca^{2+} responses elicited by physiological doses of UVR (150 mJ/cm^2; Wicks et al., 2011) are not mediated by $G\alpha_s$ or $G\alpha_{i/o}$ signaling.

The Gβγ subunit of heterotrimeric G proteins can lead to increase in intracellular Ca^{2+} levels ($[Ca^{2+}]_{ic}$) by directly activating PLCβ (Park et al., 1993; Wu et al., 1993; Barr et al., 2000). To test if UVR-mediated elevation in $[Ca^{2+}]_{ic,}$ requires activation of Gβγ, we incubated HEMs with the Gβγ-inhibiting peptide mSIRK (10 µM) or its inactive analogue L9A (10 µM; Goubaeva et al., 2003; Malik et al., 2005; Wang and Hatton, 2007) before stimulation with 150 mJ/cm^2 UVR. No significant difference was measured between UVR-induced Ca^{2+} responses in HEMs treated with mSIRK compared with the inactive analogue L9A (Fig. 1, C and D; $F_{norm,max} = 0.43 \pm 0.05$ for mSIRK vs. 0.43 ± 0.04 for L9A), which suggests Gβγ does not mediate UVR-induced Ca^{2+} responses in HEMs.

We next investigated whether members of the $G\alpha_{q/11}$ family, known to promote Ca^{2+} mobilization through PLCβ activation (Smrcka et al., 1991; Taylor et al., 1991), mediate the UVR-induced Ca^{2+} response. To alter $G\alpha_{q/11}$ signaling, we expressed RGS2 in HEMs (Heximer et al., 1997; Heximer, 2004; Roy et al., 2006), a member of the regulators of G protein signaling (RGS) family, which inactivates $G\alpha_{q/11}$ by promoting the hydrolysis of GTP to

GDP (De Vries et al., 2000). Lentiviral transduction of HA-RGS2 in HEMs resulted in the expression of a protein of the expected molecular size (Fig. S1 A) that reduced Ca^{2+} responses to activation of the $G\alpha_{q/11}$-coupled endothelin receptors endogenously present in HEMs (Yada et al., 1991; Imokawa et al., 1992; Fig. S1, B and C). Because HEMs expressing HA-RGS2 exhibited reduced $G\alpha_{q/11}$-mediated signaling via endothelin receptors, we tested if UVR-induced Ca^{2+} responses were also reduced. When compared with control transduced HEMs, cells expressing HA-RGS2 stimulated with 150 mJ/cm^2 UVR had significantly reduced retinal-dependent Ca^{2+} responses (Fig. 1, E and F; $F_{norm,max}$ = 0.62 ± 0.03 for control vs. 0.37 ± 0.06 for RGS2), which suggests that members of the $G\alpha_{q/11}$ family mediate UVR signaling in HEMs. To determine which members of the $G\alpha_{q/11}$ family are expressed in HEMs and might be activated by UVR, we examined the mRNA expression levels of $G\alpha_{q/11}$ family members $G\alpha_q$, $G\alpha_{11}$, $G\alpha_{14}$, and $G\alpha_{15}$ by qPCR. We found that in HEMs $G\alpha_q$ and $G\alpha_{11}$ are expressed at similarly high levels, whereas $G\alpha_{14}$ and $G\alpha_{15}$ are expressed at lower levels (Fig. 1 G).

Both $G\alpha_q$ and $G\alpha_{11}$ contribute to the UVR-induced Ca^{2+} response in HEMs

We investigated the contribution of $G\alpha_q$ versus $G\alpha_{11}$ to UVR signaling using RNA interference. Because $G\alpha_q$ and $G\alpha_{11}$ share a high degree of homology, we designed miRNA targeting either $G\alpha_q$ or $G\alpha_{11}$ individually, or both $G\alpha_q$ and $G\alpha_{11}$ ($G\alpha_{q/11}$). Expression of $G\alpha_q$-targeted miRNA in HEMs resulted in a significant reduction in the mRNA transcript levels of $G\alpha_q$, but not of $G\alpha_{11}$, relative to control (scrambled) miRNA-expressing cells (Fig. 2 A; $G\alpha_q$ mRNA relative to control = 0.14 ± 0.01, $G\alpha_{11}$ mRNA relative to control = 0.83 ± 0.16). Cells expressing $G\alpha_q$-targeted miRNA had a reduced Ca^{2+} response to 6 nM endothelin when compared with control miRNA-expressing cells, which suggests that

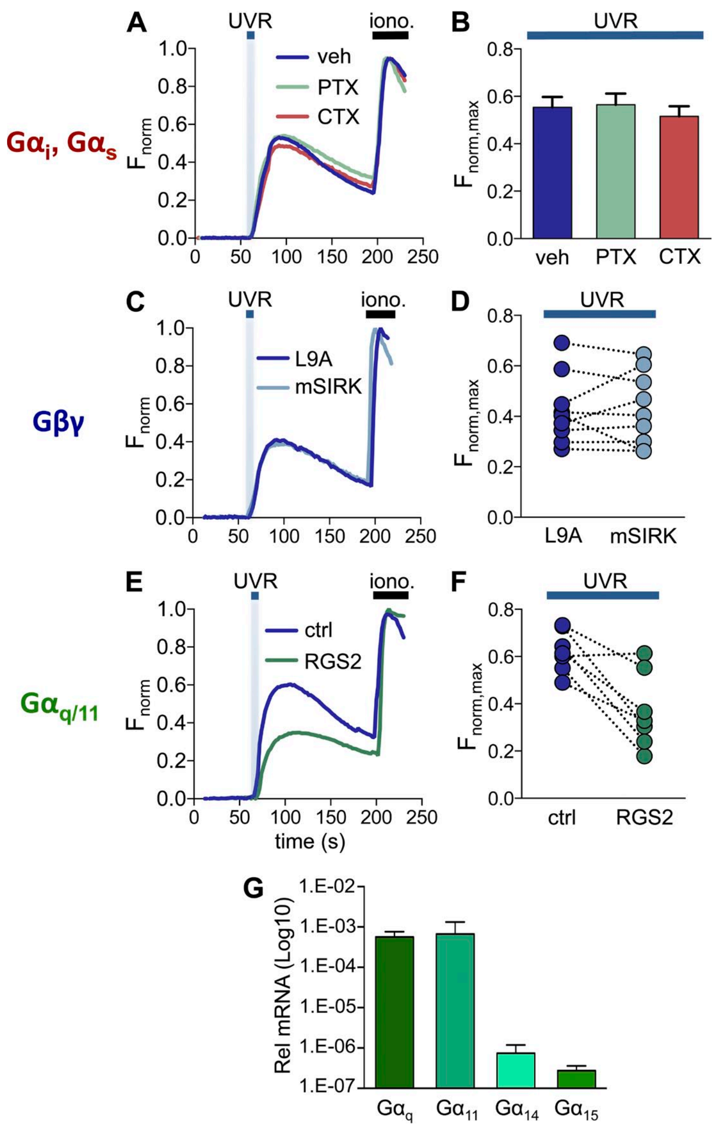

Figure 1. Impaired $G\alpha_{q/11}$ signaling, but not $G\alpha_s$, $G\alpha_{i/o}$, or $G\beta\gamma$ signaling, diminishes UVR-induced Ca^{2+} responses in HEMs. (A) HEMs treated with the $G\alpha_s$ signaling inhibitor CTX (500 ng/ml), the $G\alpha_{i/o}$ inhibitor PTX (500 ng/ml), or vehicle (water) have similar retinal-dependent Ca^{2+} responses (F_{norm}) to 150 mJ/cm^2 UVR. Each trace was normalized to the response elicited by ionomycin (iono., 1 µM), added at the end of each experiment. n = 7–10 cells from one experiment averaged for each trace. (B) The mean peak Ca^{2+} responses ($F_{norm,max}$) elicited by 150 mJ/cm^2 UVR were not altered when HEMs were treated with CTX or PTX, as compared with vehicle control. n = 7 experiments per condition, ±SEM (error bars). (C) HEMs stimulated with 150 mJ/cm^2 UVR and treated with the $G\beta\gamma$ peptide inhibitor mSIRK (10 µM) or its inactive analogue L9A (10 µM) had similar retinal-dependent Ca^{2+} responses (F_{norm}). n = 6–10 cells from one experiment averaged for each trace. (D) Mean UVR-induced (150 mJ/cm^2) peak retinal-dependent Ca^{2+} responses ($F_{norm,\ max}$) were not significantly different in HEMs treated with the $G\beta\gamma$ peptide inhibitor mSIRK versus its inactive analogue L9A. n = 9 paired experiments. (E) HEMs expressing RGS2 exhibited reduced retinal-dependent Ca^{2+} responses (F_{norm}) to 150 mJ/cm^2 UVR compared with control (mCherry-transfected) cells. n = 3–11 cells from one experiment averaged for each trace. (F) In paired experiments the mean amplitude of the retinal-dependent Ca^{2+} responses ($F_{norm,max}$) in RGS2-expressing HEMs stimulated with UVR (150 mJ/cm^2) was diminished compared with control cells. n = 8 experiments per condition, $P < 0.004$. (G) qPCR analysis of mRNA levels of $G\alpha_{q/11}$ family members ($G\alpha_q$, $G\alpha_{14}$, $G\alpha_{14}$, and $G\alpha_{15}$) in HEMs, relative to actin. Bars represent mean ± SEM (error bars) from n = 3 independent experiments.

Gα$_q$-targeted miRNA significantly reduced Gα$_q$ signaling (Fig. S2, A and B). We then measured retinal-dependent Ca^{2+} responses elicited by 150 mJ/cm^2 UVR and found that HEMs expressing Gα$_q$-targeted miRNA had significantly reduced Ca^{2+} responses compared with HEMs expressing control miRNA (Fig. 2, B and C; $F_{norm,max}$ = 0.57 ± 0.04 for control miRNA, 0.35 ± 0.03 for Gα$_q$ miRNA).

Expression of Gα$_{11}$-targeted miRNA resulted in a significant reduction in the mRNA levels of Gα$_{11}$ (Gα$_{11}$ mRNA relative to control = 0.12 ± 0.03) and a smaller decrease in the mRNA transcript levels of Gα$_q$ (Fig. 2 D; Gα$_q$ mRNA relative to control = 0.75 ± 0.07). HEMs expressing Gα$_{11}$-targeted miRNA had reduced Ca^{2+} responses to 6 nM endothelin (Fig. S2, C and D), which suggests that Gα$_{11}$ signaling is also reduced. In response to stimulation with 150 mJ/cm^2 UVR, HEMs expressing Gα$_{11}$-targeted miRNA had a reduced retinal-dependent Ca^{2+} response compared with HEMs expressing control miRNA ($F_{norm,max}$ = 0.61 ± 0.04 for control miRNA, 0.40 ± 0.05 for Gα$_{11}$ miRNA; Fig. 2, E and F). Collectively, our data from HEMs expressing Gα$_q$ or Gα$_{11}$-targeted

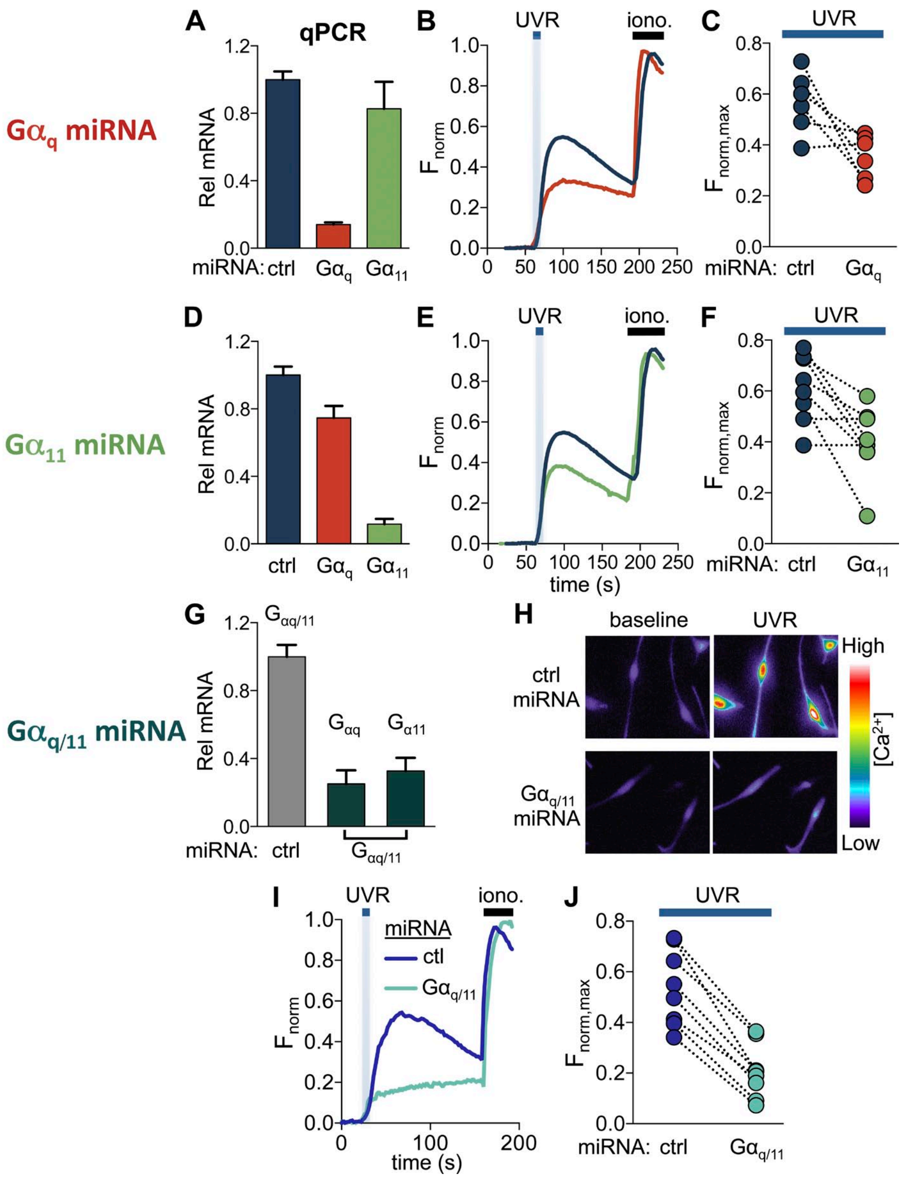

Figure 2. Gα$_q$ and Gα$_{11}$ signaling contribute to UVR-induced Ca^{2+} responses. (A) HEMs expressing Gα$_q$-targeted miRNA had significantly reduced (~85%) Gα$_q$ levels, but not Gα$_{11}$ mRNA levels compared with control miRNA-expressing cells (ctrl). n = 4 experiments, $P < 0.0001$, ±SEM (error bars). (B) Retinal-dependent Ca^{2+} responses (F_{norm}) to 150 mJ/cm^2 UVR were reduced in HEMs expressing Gα$_q$-targeted versus control miRNA. Each trace represents the average of 5–10 cells from one experiment. (C) In paired experiments, HEMs expressing Gα$_q$-targeted miRNA had reduced mean peak retinal-dependent Ca^{2+} responses ($F_{norm,max}$) compared with control miRNA-expressing HEMs. n = 6 experiments per condition, $P < 0.009$. (D) HEMs expressing Gα$_{11}$-targeted miRNA had Gα$_{11}$ mRNA levels reduced by ~90% and Gα$_q$ transcript levels reduced by ~20%, compared with control miRNA-expressing cells. n = 4 experiments, ±SEM (error bars). (E) Retinal-dependent Ca^{2+} responses (F_{norm}) induced by 150 mJ/cm^2 UVR were reduced in HEMs expressing Gα$_{11}$-targeted miRNA relative to control miRNA-expressing cells. Each trace represents the average of 3–10 cells from one experiment. (F) HEMs expressing Gα$_{11}$-targeted miRNA elicited smaller mean peak retinal-dependent Ca^{2+} responses ($F_{norm,max}$) compared with control miRNA-expressing cells. n = 8, $P < 0.008$. (G) miRNA targeting a conserved region of Gα$_q$ and Gα$_{11}$ (Gα$_{q/11}$) reduced the mRNA transcript levels of Gα$_q$ by ~75% and of Gα$_{11}$ by ~70%, relative to control miRNA-expressing cells. n = 4, ±SEM (error bars). (H) Pseudochrome fluorescence images of HEMs loaded with Ca^{2+} indicator and preincubated with retinal. (H, top) Images of HEMs expressing control miRNA recorded before UVR stimulation (baseline) and at the peak of the Ca^{2+} response to 150 mJ/cm^2 UVR (UVR). (H, bottom) Images of HEMs expressing Gα$_{q/11}$-targeted miRNA before UVR stimulation (baseline) and at the peak of the UVR-induced Ca^{2+} response (UVR). HEMs expressing Gα$_{q/11}$-targeted miRNA showed a reduced fluorescence response to UVR compared with control miRNA (bottom vs. top UVR). (I) HEMs expressing Gα$_{q/11}$-targeted miRNA had reduced retinal-dependent Ca^{2+} responses evoked by 150 mJ/cm^2 UVR compared with HEMs expressing control miRNA. Each trace represents the average of n = 4–10 cells from one experiment. (J) The mean peak UVR-induced Ca^{2+} response measured in paired experiments in HEMs expressing Gα$_{q/11}$-targeted miRNA was reduced compared with control miRNA. n = 8, $P < 0.0001$.

miRNA suggest that both $G\alpha_q$ and $G\alpha_{11}$ contribute to the UVR-induced retinal-dependent phototransduction pathway in HEMs.

We next examined if decreasing $G\alpha_q$ and $G\alpha_{11}$ levels simultaneously had a larger effect on UVR-induced Ca^{2+} responses in HEMs. Expression of $G\alpha_{q/11}$ miRNA that targets both $G\alpha_q$ and $G\alpha_{11}$ significantly reduced the mRNA levels of $G\alpha_q$ and $G\alpha_{11}$ relative to control miRNA-expressing cells (Fig. 2 G; $G\alpha_q$ mRNA relative to control = 0.24 ± 0.08, $G\alpha_{11}$ mRNA relative to control = 0.32 ± 0.08). Stimulation with 6 nM endothelin resulted in reduced Ca^{2+} responses in HEMs expressing $G\alpha_{q/11}$-targeted compared with control miRNA (Fig. S2 E and Fig. 2 F; $F_{norm,max}$ = 0.72 ± 0.04 for control miRNA, 0.44 ± 0.07 for $G\alpha_{q/11}$ miRNA). UVR stimulation of HEMs expressing $G\alpha_{q/11}$-targeted miRNA led to smaller increases in intracellular Ca^{2+} levels compared with control miRNA-treated cells (Fig. 2 H). Quantification of these responses showed that the UVR-induced Ca^{2+} responses were significantly reduced in the presence of $G\alpha_{q/11}$-targeted miRNA compared with control miRNA (Fig. 2, I and J), which suggests that both subunits $G\alpha_q$ and $G\alpha_{11}$ contribute to retinal-dependent UVR-induced Ca^{2+} responses in HEMs.

UVR stimulation of HEMs leads to activation of a whole-cell current mediated by TRPA1 ion channels in a retinal and G protein–dependent manner (Bellono et al., 2013). We thus investigated if $G\alpha_{q/11}$ is also required for UVR-induced whole-cell currents. We first tested the effect of $G\alpha_{q/11}$-targeted miRNA on whole-cell currents measured at +80 mV in response to 240 mJ/cm^2 UVR and found that expression of control miRNA had no effect on the photocurrents, whereas $G\alpha_{q/11}$-targeted miRNA nearly abolished them (Fig. 3, A and B; $I_{UVR/ctrl\ miRNA}$ = 4.06 ± 0.29 pA/pF, $I_{UVR/\ G\alpha q/11\ miRNA}$ = 0.28 ± 0.17 pA/pF) at all voltages (Fig. 3 B, inset). The whole-cell patch clamp technique used to measure the photocurrents allowed us to use an alternative method to block $G\alpha_{q/11}$ signaling by dialyzing GPAnt-2a, a $G\alpha_{q/11}$ inhibitory peptide, into HEMs (Mukai et al., 1992). The time-dependent effect of peptide inhibitor dialysis allowed us to measure the UVR-induced current at 2 min after break-in, when the peptide was not effective, and thus the measurement was used as control, and at 10 min of dialysis, when the peptide became effective. This experimental protocol allowed us to compare the effects of the peptide inhibitors in the same cell. When GPAnt-2a was included in

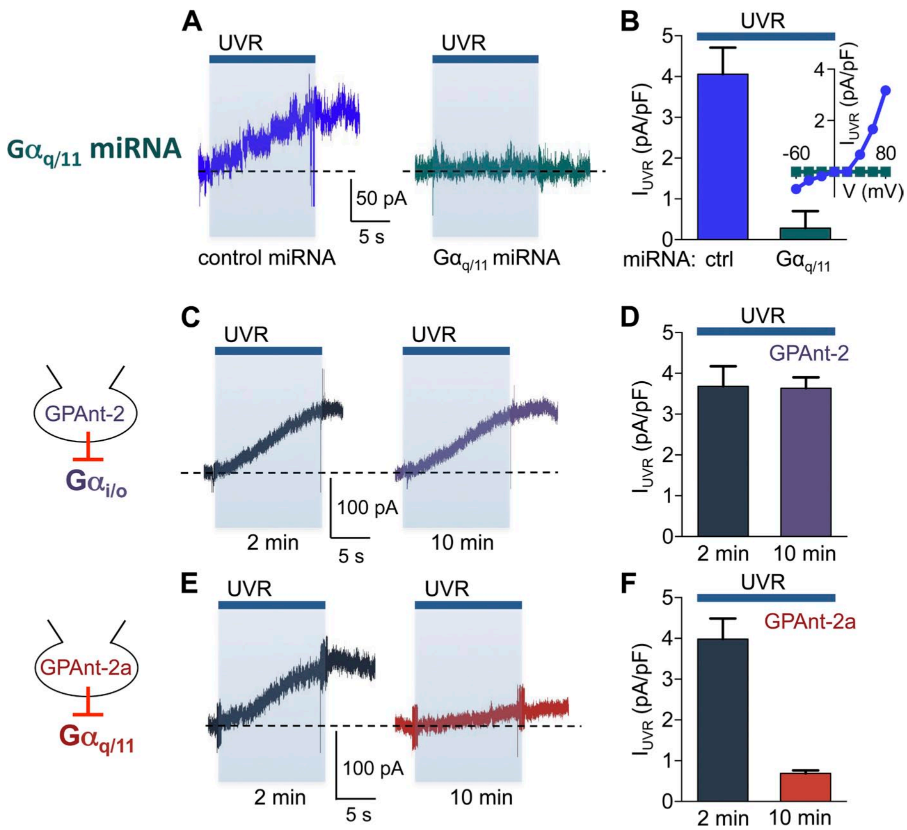

Figure 3. $G\alpha_{q/11}$ mediates the retinal-dependent UVR photocurrent in HEMs. (A) Expression of $G\alpha_{q/11}$-targeted miRNA in a representative HEM abolished the UVR (240 mJ/cm^2)-induced whole-cell current at +80 mV exhibited in cells expressing control miRNA. Recordings were performed from two populations of cells: one expressing control miRNA and the other expressing $G\alpha_{q/11}$-targeted miRNA. (B) HEMs expressing $G\alpha_{q/11}$-targeted miRNA had an ∼93% lower mean peak UVR photocurrent density compared with those expressing control miRNA. n = 8 cells per condition, $P < 0.0001$, ±SEM (error bars). (B, inset) UVR-induced increase in current density versus voltage in a representative HEM-expressing control or $G\alpha_{q/11}$-targeted miRNA. (C) $G\alpha_i$/$G\alpha_o$ signaling inhibitor peptide GPAnt-2 (40 µM) did not affect the UVR photocurrents after 10 min of patch pipette dialysis in a representative HEM (traces from the same cell). (D) The mean peak UVR photocurrent density was similar when GPAnt-2 (40 µM) was included in the patch pipette and HEMs were stimulated with UVR 2 or 10 min after break-in. n = 6 cells per condition. Error bars indicate ±SEM. (E) $G\alpha_{q/11}$ signaling inhibitor peptide GPAnt-2a significantly reduced the UVR photocurrent after 10 min compared with 2 min of patch pipette dialysis in a representative HEM (traces from the same cell). The broken horizontal lines represent the baseline current for each recording. (F) The mean peak UVR photocurrent was reduced by ∼83% in HEMs dialyzed with GPAnt-2a for 10 min, compared with 2 min. n = 6 cells per condition, $P < 0.0001$, ±SEM (error bars).

the pipette solution, the UVR photocurrents were similar to control cells 2 min after break-in, but decreased significantly after 10 min of dialysis (Fig. 3, E and F; $I_{UVR/GPAnt\text{-}2a}$ = 3.98 ± 0.50 pA/pF at 2 min, 0.69 ± 0.08 pA/pF after 10 min of dialysis with GPAnt-2a). As a control we performed a similar experiment using the GPAnt-2 peptide, which inhibits $G\alpha_{i/o}$ signaling (Mukai et al., 1992), and detected no change in the amplitude of the UVR current after 2 or 10 min of dialysis (Fig. 3, C and D; $I_{UVR/GPAnt\text{-}2}$ = 3.68 ± 0.49 pA/pF at 2 min, 3.64 ± 0.26 pA/pF after 10 min). These results suggest that UVR-induced photocurrents are dependent on $G\alpha_{q/11}$ signaling.

UVR-activated TRPA1 photocurrents are regulated by PIP_2 in HEMs

Our results so far indicate that UVR phototransduction leads to activation of $G\alpha_{q/11}$, which in turn activates PLCβ, required both for intracellular Ca^{2+} release (Wicks et al., 2011) and TRPA1 activation (Bellono et al., 2013). Nonetheless, the mechanism by which UVR leads to TRPA1 activation downstream of PLCβ remains unknown. Because PLCβ hydrolyzes plasma membrane PIP_2, generating DAG and the soluble messenger IP_3, we reasoned that PLCβ-dependent signaling could modulate TRPA1 channel activity in HEMs via IP_3, DAG, or PIP_2.

We first tested whether IP_3 or IP_3-mediated Ca^{2+} release was sufficient to activate TRPA1 by using a control internal solution, allowing for an increase in $[Ca^{2+}]_{ic}$ (see Materials and methods), internal solutions containing 100 µM IP_3 to stimulate IP_3Rs, or 1 mg/ml heparin to block IP_3Rs, with both treatments occluding subsequent UVR-induced IP_3R-mediated Ca^{2+} release. UVR (240 mJ/cm^2) exposure after dialysis for 5 min with each of the three solutions elicited retinal-dependent photocurrents with similar amplitudes (Fig. S3, A and B; $I_{UVR/Ctrl}$ = 4.01 ± 0.33 pA/pF, $I_{UVR/IP3}$ = 4.04 ± 0.47 pA/pF, $I_{UVR/heparin}$ = 5.05 ± 0.56 pA/pF), which suggests that UVR-induced activation of whole-cell currents is not mediated by IP_3 or IP_3R-mediated Ca^{2+} release.

We next examined the contribution of DAG to retinal-dependent UVR photocurrents. Bath application of the PC-PLC (10 U/ml), which generates DAG in the plasma membrane (Oancea et al., 1998), or of the DAG analogue OAG (100 µM), did not elicit a significant current in HEMs, and 5 min of incubation with the respective treatments did not affect the retinal-dependent photocurrents elicited by UVR (Fig. S3, C and D; $I_{PC\text{-}PLC}$ = 0.10 ± 0.10 pA/pF, I_{OAG}= 0.20 ± 0.09 pA/pF, $I_{UVR/PC\text{-}PLC}$ = 4.31 ± 0.70 pA/pF, $I_{UVR/OAG}$ = 4.13 ± 0.48 pA/pF). Because increasing DAG levels failed to elicit whole-cell currents and had no effect on UVR photocurrents, we concluded that DAG does not modulate TRPA1 downstream of UVR.

PIP_2 hydrolysis is a key regulator for many ion channels (Suh and Hille, 2005), including TRPA1 (Dai et al., 2007; Karashima et al., 2008; Kim et al., 2008). To test if the presumed decrease in PIP_2 levels caused by PLCβ-mediated hydrolysis affects UVR photocurrents, we attempted to maintain elevated PIP_2 levels by dialyzing HEMs with the PIP_2 analogue diC8-PIP_2 (20 µM; Karashima et al., 2008; Kim et al., 2008). We found that after 5 min of patch pipette dialysis to allow diC8-PIP_2 to diffuse into cells, UVR stimulation (240 mJ/cm^2) elicited significantly smaller photocurrents at all voltages compared with UVR photocurrents measured immediately after break-in (Fig. 4, A, B, and D). This finding suggests that increased PIP_2 prevents UVR-induced TRPA1 activation and raises the question of whether PIP_2 hydrolysis is required for the UVR photocurrent.

To test if the dialysis with diC8-PIP_2 inhibited TRPA1, or another component of the UVR phototransduction cascade, we compared the whole-cell currents elicited by UVR and the TRPA1 agonist cinnamaldehyde (CA) in HEMs dialyzed with diC8-PIP_2 or GPAnt-2a (Fig. S4). We found that dialysis with both diC8-PIP_2 and GPant-2a inhibited UVR photocurrents, whereas only diC8-PIP_2 inhibited currents elicited by CA (Fig. S4). These data suggest that GPAnt-2a inhibits an important component of the UVR signaling cascade, $G\alpha_{q/11}$, while diC8-PIP_2 directly inhibits TRPA1 activity, which is required for both the UVR- and CA^{2+}-elicited increase in whole-cell current.

To test if a decrease in PIP_2 levels is also sufficient to cause TRPA1 activation in HEMs, we dialyzed cells with polylysine (polyK; 50 mg/ml), which binds and sequesters PIP_2 (Lukacs et al., 2007; Klein et al., 2008; Ufret-Vincenty et al., 2011), preventing it from acting on the TRPA1 channels. A subsaturating UVR dose (160 mJ/cm^2; Bellono et al., 2013) evoked a submaximal UVR photocurrent in HEMs dialyzed with control internal solution. PolyK alone, when included in the pipette solution and allowed to diffuse into the cell and sequester PIP_2, did not lead to an increase in whole-cell current; however, it significantly enhanced UVR photocurrents elicited by the same subsaturating UVR dose (Fig. 4, C and E; I_{PolyK} = 0.07 ± 0.03 pA/pF, $I_{UVR/Ctrl}$ = 2.51 ± 0.07 pA/pF, $I_{UVR/PolyK}$ = 4.90 ± 0.44 pA/pF). The polyK-modulated UVR photocurrent was inhibited by the TRPA1 antagonist HC-030031 (HC; 100 µM; Fig. 4 C, right; and Fig. 4 E; $I_{UVR/PolyK+HC}$ = 0.27 ± 0.12 pA/pF), which suggests that the enhanced photocurrent was mediated by TRPA1.

To address the specificity of the phospholipids that modulate the UVR photocurrents, we used recombinant pleckstrin homology (PH) domains from phospholipase C δ1 (PLCδ1-PH) that selectively bind PIP_2 and from the general receptor for phosphoinositides type 1 (GRP1-PH) that selectively binds PI(3,4,5)P_3 (PIP_3; Klein et al., 2008). Dialysis of recombinant PH domains in HEMs will bind and sequester the phosphoinotides, resulting in decreased cellular levels. When PLCδ1-PH was included in the pipette, a significantly enhanced photocurrent was elicited by a subsaturating UVR dose (160 mJ/cm^2), compared with boiled PLCδ1-PH or GRP1-PH (Fig. 4, F and G; $I_{PLC\delta 1\text{-}PH}$ = 3.01 ± 0.36 pA/pF, $I_{Boiled\ PLC\delta 1\text{-}PH}$ = 1.32 ± 0.26 pA/pF, $I_{GRP1\text{-}PH}$ = 1.34 ± 0.24 pA/pF). These results suggest that sequestering PIP_2, but not PIP_3, levels in HEMs leads to increased TRPA1 activity in response to UVR, leading us to hypothesize that UVR-mediated PIP_2 hydrolysis releases the PIP_2-mediated inhibition of TRPA1.

IP_3R and TRPA1 mediate UVR-induced Ca^{2+} responses and regulate Ca^{2+} signaling kinetics

Retinal-dependent UVR-induced Ca^{2+} responses triggered downstream of $G\alpha_{q/11}$ signaling are mediated by two sources of Ca^{2+}: (1) efflux from intracellular thapsigargin-sensitive stores and (2) influx via TRPA1 at the plasma membrane (Bellono et al., 2013). Because $G\alpha_{q/11}$/PLCβ signaling generates the second messenger IP_3, we hypothesized that IP_3Rs mediate Ca^{2+} release from intracellular stores. To test this hypothesis, we treated HEMs with the IP_3R antagonist XeC (25 µM; Gafni et al., 1997; Oka et al., 2002) and found that UVR-induced Ca^{2+} responses were significantly reduced (Fig. 5, A and B). To study the contribution of each Ca^{2+} source (IP_3R vs. TRPA1) to the overall response, we measured Ca^{2+} responses in HEMs preincubated with XeC in order to inhibit IP_3R, or HC-030031 (HC; 100 µM) in order to inhibit TRPA1 (Fig. 4 A). Ca^{2+} responses elicited by 240 mJ/cm^2 UVR were reduced by 71% in the presence of XeC, by ~45% in the presence of HC, and by ~90% in the presence of both antagonists, as compared with vehicle-treated cells (Fig. 4 B; fluorescence increase over baseline: $\Delta F/F_o$ = 3.21 ± 0.27 for vehicle, 0.94 ± 0.16 for XeC, 1.77 ± 0.29 for HC, and 0.34 ± 0.07

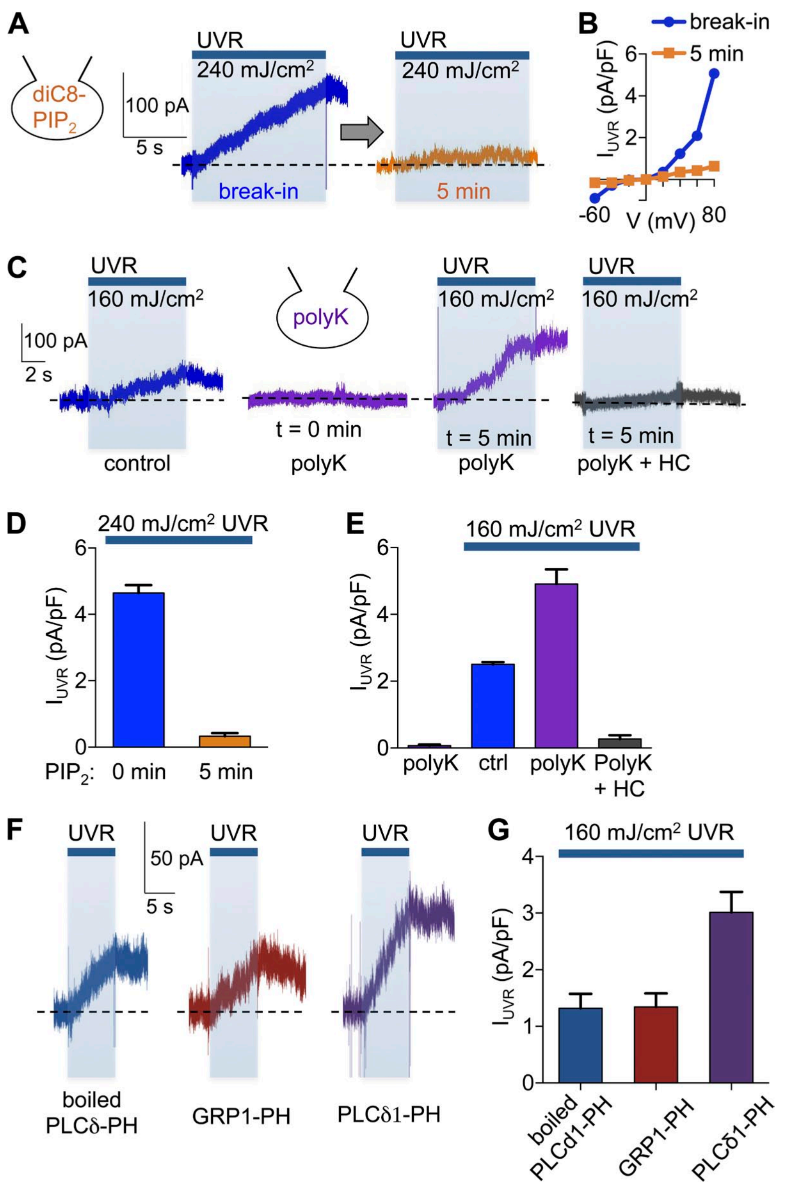

Figure 4. PIP_2 regulates UVR-activated TRPA1 currents. (A) The UVR (240 mJ/cm^2)-induced whole-cell current of a representative HEM dialyzed with the PIP_2 analogue diC8-PIP_2 and measured at +80 mV immediately after break-in was significantly reduced after 5 min of dialysis to allow diC8-PIP_2 to diffuse into the cell. (B) HEMs dialyzed with diC8-PIP2 had reduced UVR photocurrent densities at all voltages when stimulated after 5 min of dialysis, compared with immediately after break-in. (C) HEMs exposed to a submaximal UVR dose (160 mJ/cm^2) elicited a small but significant increase in whole-cell current at +80 mV (first trace). Including poly-lysine (polyK, 50 mg/ml) in the patch pipette did not alter the baseline current, but significantly potentiated the UVR (160 mJ/cm^2)-induced current after 5 min of dialysis (second and third trace from the same representative cell). The augmented UVR-induced current measured in the presence of polyK was abolished by treatment with the TRPA1 antagonist HC-030031 (HC; 100 µM; fourth trace). (D) Dialysis with diC8-PIP_2 reduced mean peak UVR photocurrents by ~93% compared with control. n = 7 cells, $P < 0.0001$, ±SEM (error bars). (E) PolyK dialysis did not elicit a significant increase in mean current density in the absence of UVR stimulation, but increased retinal-dependent photocurrents induced by 160 mJ/UVR by ~96%. This effect was abolished by HC. n = 6 cells per condition, $P < 0.0008$, ±SEM (error bars). (F) The UVR photocurrent induced by 160 mJ/cm^2 UVR in a representative HEM was enhanced after 7 min of dialysis with PLCδ-PH (60 µM), when compared with boiled PLCδ-PH (60 µM) or GRP1-PH (60 µM). The broken horizontal lines represent the baseline current for each recording. (G) Dialysis of HEMs with PLCδ1-PH (60 µM) enhanced mean peak UVR photocurrents by ~128% compared with cells dialyzed with boiled PLCδ1-PH (60 µM) or GRP1-PH (60 µM). n = 7–8 cells per condition, $P < 0.002$, ±SEM (error bars).

for XeC + HC). These results suggest that UVR phototransduction evokes a rise in $[Ca^{2+}]_{ic}$ via intracellular Ca^{2+} release from IP_3R and Ca^{2+} influx through TRPA1 ion channels.

We next sought to distinguish the contribution of each Ca^{2+} source (IP_3R and TRPA1) to the biphasic nature of the transient UVR-induced Ca^{2+} response. To do that, we measured the initial slope and the decay time constant of Ca^{2+} responses in HEMs treated with XeC or HC, compared with vehicle. The mean initial slope of UVR-induced Ca^{2+} responses (measured during the first 30 s after the beginning of UVR stimulation) was reduced by ∼76% with XeC treatment and by ∼35% with HC treatment when compared with vehicle-treated HEMs (Fig. 5, C and D; $\Delta F/s = 0.100 \pm 0.009$ for vehicle, 0.024 ± 0.003 for XeC, and 0.064 ± 0.01 for HC). These results suggest that both sources contribute to the initial rising phase of the Ca^{2+} response, but IP_3-mediated Ca^{2+} release has a significantly greater contribution.

The time constant for the decay phase (τ_{off}) of the UVR-induced Ca^{2+} response was measured by monitoring cellular Ca^{2+} levels for ≥200 s after the peak of the response in cells treated with XeC, HC, or vehicle. HEMs treated with XeC had Ca^{2+} responses with mean τ_{off} values ∼79% higher than vehicle-treated cells, which suggests that the IP_3-mediated response decays on a fast time scale. Interestingly, treatment with HC

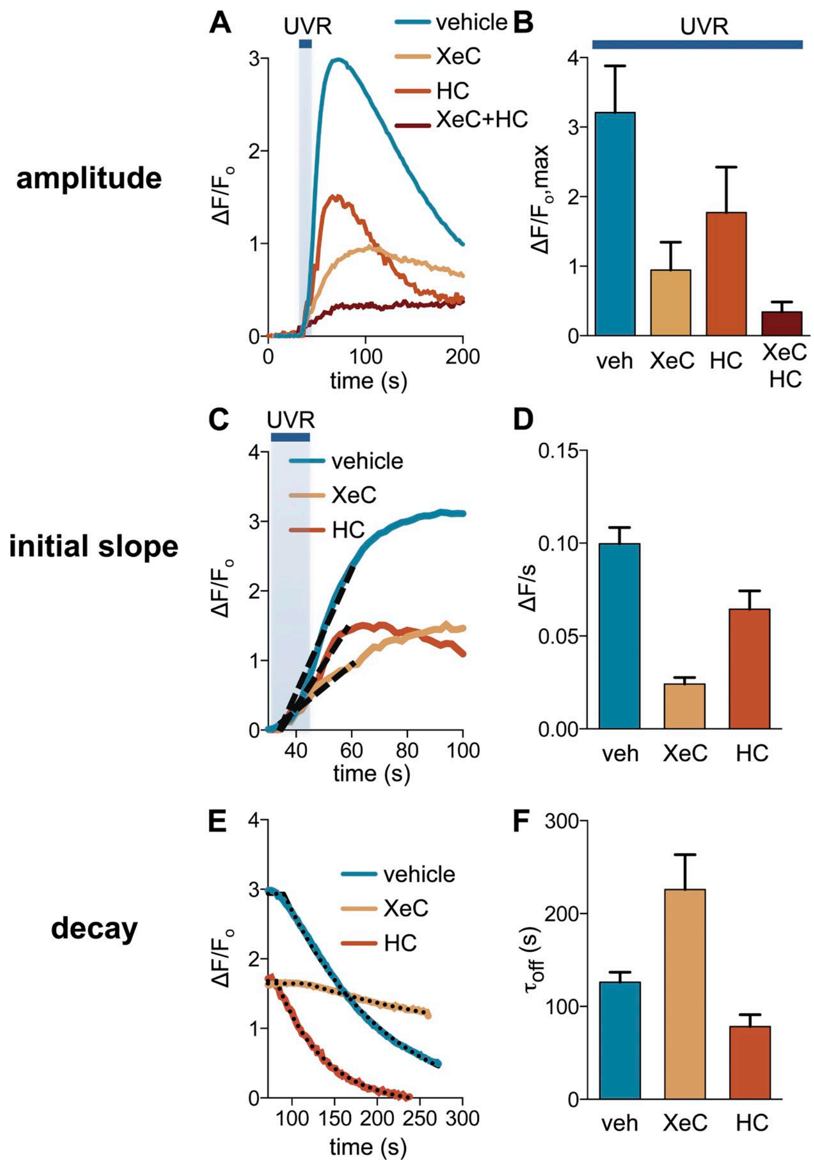

Figure 5. IP_3R and TRPA1 activity mediate UVR-induced Ca^{2+} responses and regulate signaling kinetics. (A) In HEMs the amplitudes of the retinal-dependent Ca^{2+} responses induced by 240 mJ/cm^2 UVR in the presences of vehicle (1% DMSO) were reduced by the IP_3R antagonist XeC (25 µM) and the TRPA1 antagonist HC-030031 (HC; 100 µM), and further reduced in the presence of both XeC and HC. *n* = 10–15 cells per condition. (B) Mean peak UVR-induced Ca^{2+} responses in the presence of vehicle were reduced by ∼71% in the presence of XeC, by ∼45% in the presence of HC, and by ∼90% by the coapplication of XeC and HC, respectively. *n* = 6 experiments per condition. $P < 0.0001$ for XeC versus control, $P < 0.007$ for HC versus control, $P < 0.0001$ for XeC + HC versus control, ±SEM (error bars). (C) Analysis of the first 30 s of the UVR-induced Ca^{2+} response showed that treatment with XeC or HC reduced the initial slope compared to vehicle control. *n* = 10–15 cells from one experiment per condition. The broken lines represent the slopes of the initial increase in calcium (the straight line that fits the initial phase of the calcium response curve). The tangents of the angles formed by these lines with the x axis are represented in D ($\Delta F/s$). (D) The mean initial slope of the Ca^{2+} response measured during the first 30 s after the beginning of UVR stimulation was reduced by ∼76% when cells were treated with XeC and by ∼35% when cells were treated with HC, compared with vehicle-treated cells. *n* = 6 experiments per condition. $P < 0.0001$ for XeC versus control, $P < 0.03$ for HC versus control, ±SEM (error bars). (E) The decay of the UVR-induced Ca^{2+} response (τ_{off}), calculated by fitting the responses with a single exponential, was significantly longer in HEMs treated with XeC and reduced in HEMs treated with HC, compared with vehicle-treated cells. *n* = 10–15 cells per condition. The broken lines represent the exponential curve that fits the decreasing part of the calcium response shown in A. The exponential coefficient of these curves represents τ_{off}, shown in F. (F) The mean τ_{off} of UVR-induced Ca^{2+} response decay in HEMs treated with vehicle was increased by ∼79% in the presence of XeC and reduced by ∼38% in the presence of HC. *n* = 6 experiments per condition. $P < 0.03$ for XeC versus control, $P < 0.03$ for HC versus control, ±SEM (error bars).

resulted in UVR-evoked Ca^{2+} responses that decayed ~38% faster than vehicle-treated cells (Fig. 5, E and F; τ_{off} = 225.90 ± 37.44 s for XeC, 78.42 ± 12.68 s for HC, and 126.20 ± 10.61 s for vehicle). Hence, TRPA1 activation extends the duration of the Ca^{2+} responses, whereas IP_3R activation reduces the duration. Collectively, our results suggest that IP_3R-mediated Ca^{2+} release is important to ensure a fast rising phase of the response. In contrast, consistent with our previous findings (Bellono and Oancea, 2013; Bellono et al., 2013), TRPA1 activation is slow but persistent, contributing to a prolonged Ca^{2+} response (Fig. 6 B).

DISCUSSION

We have recently discovered that primary human melanocytes are capable of rapidly detecting UVR by first increasing intracellular Ca^{2+} and later producing more melanin (Wicks et al., 2011). The Ca^{2+} response is retinal dependent and is in part due to calcium release from intracellular stores and in part to calcium influx through TRPA1 ion channels (Bellono et al., 2013). Both components of the response require heterotrimeric G proteins and PLCβ activation (Wicks et al., 2011; Bellono et al., 2013). Here we investigated the identity of the G protein subunit that mediates the response and found that reducing the expression of both $G\alpha_q$ and $G\alpha_{11}$, as well as using a peptide that inhibits $G\alpha_{q/11}$ signaling, significantly decreased both components of the Ca^{2+} response (Figs. 2 and 3). These results suggest that the UVR-activated pathway is mediated by $G\alpha_{q/11}$, which, in turn, activates PLCβ.

Signal transduction pathways associated with G protein activation often result in modulation of TRP ion channels. For example, in *Drosophila*, light stimulation of rhodopsin results in activation of $G\alpha_{q/11}$ and PLCβ, which hydrolyzes PIP_2 to produce DAG and IP_3, to regulate TRP ion channels (Hardie, 2001). We reasoned that one of these messengers (IP_3, DAG, or PIP_2) might regulate the UVR-activated TRPA1 photocurrent and tested our hypothesis by exogenously altering the levels of these messengers (Figs. 4 and S3). We found that reagents used to manipulate the levels of IP_3 and DAG had no effect on the photocurrent, whereas reagents that affect PIP_2 levels did. Allowing diC8-PIP_2 to diffuse into the cell blocked the current in response to a UVR dose that evokes a maximal response, which suggests that decreasing PIP_2 levels is a necessary step in TRPA1 activation. But is the decrease in PIP_2 sufficient to activate TRPA1?

Sequestration of PIP_2 using polyK did not elicit a significant current in the absence of UVR, but did potentiate TRPA1 currents evoked by UVR. Furthermore, using PLCδ1-PH to specifically sequester PIP_2 enhanced UVR photocurrents, whereas sequestration of PIP_3 by GRP1-PH had no effect. These results suggest that a decrease in PIP_2 can modulate the photocurrent, but may not be sufficient for TRPA1 activation. Therefore, other messengers or proteins that contribute to the phototransduction pathway could be involved. Our results add to the already controversial role of PIP_2 in modulating TRPA1. PIP_2 was found to potentiate agonist-activated TRPA1 currents (Karashima et al., 2008), but also to inhibit TRPA1 activity (Dai et al., 2007; Kim et al., 2008). GPCRs that activate $G\alpha_{q/11}$ (bradykinin, PAR2, and Mrgprs) can regulate TRPA1, but the mechanism is unclear (Bandell et al., 2004; Dai et al., 2007; Wang et al., 2008; Wilson et al., 2011). It remains to be determined in future experiments whether PIP_2 directly interacts with TRPA1 to modulate its activity and what other cellular messengers contribute to TRPA1 activation in response to UVR and to $G\alpha_{q/11}$-coupled receptors.

Examining the relative contribution of UVR-induced IP_3R- and TRPA1-mediated Ca^{2+} responses revealed that IP_3-mediated Ca^{2+} release is rapid, but also declines fast. In contrast, TRPA1-mediated influx is slower to increase intracellular Ca^{2+}, as suggested by the slow time course of the photocurrent activation, and slow to decay, allowing intracellular Ca^{2+} to remain elevated after UVR exposure, a necessary step for melanin production (Bellono et al., 2013). However, there is a discrepancy between the time course of photocurrents and that of Ca^{2+} responses. UVR photocurrents recorded under voltage-clamp conditions peak during or shortly after light stimulation, whereas Ca^{2+} responses measured in intact cells, in which the membrane voltage could

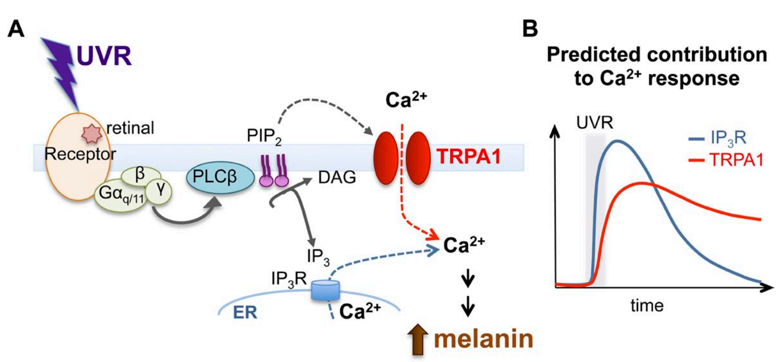

Figure 6. Proposed mechanism for the UVR phototransduction cascade in HEMs. (A) UVR stimulates a G protein–coupled receptor in a retinal-dependent manner, and leads to activation of $G\alpha_{q/11}$ and PLCβ, which hydrolyzes PIP_2 into DAG and IP_3. PIP_2 hydrolysis regulates the activity of TRPA1 at the plasma membrane to mediate Ca^{2+} influx, whereas IP_3 activates IP_3R to mediate Ca^{2+} release from intracellular stores. The increase in intracellular Ca^{2+} leads to early melanin synthesis. (B) Predicted contribution of IP_3R- and TRPA1-mediated Ca^{2+} responses to UVR-induced Ca^{2+} signaling kinetics. IP_3R contributes to the rapid initial increase in Ca^{2+}, whereas TRPA1 contributes to sustained Ca^{2+} influx.

change, peak seconds after irradiation. We recently found that UVR phototransduction depolarizes the plasma membrane of melanocytes to delay TRPA1 inactivation and prolong Ca^{2+} responses (Bellono and Oancea, 2013), a finding consistent with the TRPA1-mediated influx kinetics found in this study. The discrepancy between the time course of the response measured by the two methods is likely to be caused by the significant effects of membrane depolarization on the TRPA1 channel and consequent Ca^{2+} signaling dynamics. Our analyses of Ca^{2+} response dynamics also revealed the possibility of cross-talk between the Ca^{2+} release and influx pathways. Inhibition of IP_3R resulted in a significantly slower decline of the TRPA1-mediated Ca^{2+} response, which suggests that the IP_3-mediated response decays considerably faster than the overall response. However, when TRPA1 was inhibited, the decay of the IP_3-mediated Ca^{2+} responses was only slightly (although significantly) faster, which suggests that Ca^{2+} release may accelerate TRPA1 inactivation.

Based on our data, we propose that UVR exposure of HEMs stimulates a retinal-dependent $G\alpha_{q/11}$-coupled receptor, which activates PLCβ. Active PLCβ hydrolyzes plasma membrane PIP_2 into DAG and IP_3. Soluble IP_3 binds IP_3Rs in the ER, resulting in Ca^{2+} release, whereas the decrease in PIP_2 levels modulates TRPA1 activation and Ca^{2+} influx (Fig. 6). Our model for UVR signal transduction in human melanocytes resembles visual phototransduction in *Drosophila* photoreceptors (Hardie, 2001) and nonvisual phototransduction in the mammalian retina (Berson et al., 2002; Graham et al., 2008). The melanocyte UVR pathway also shares many similarities with a recently described UVR-activated signaling mechanism in *Drosophila* larvae, which is mediated by Ca^{2+} signals resulting from $G\alpha_{q/11}$ and TRPA1 activation (Xiang et al., 2010). The receptor for the *Drosophila* larvae UVR pathway appears to be a gustatory GPCR (Gr28b); how light can activate such a receptor remains unknown.

One of the remaining questions for the UVR phototransduction cascade in melanocytes is the identity of the receptor. The retinal dependence and G protein involvement suggests the involvement of an opsin GPCR. We previously found that rhodopsin expression contributes to UVR-induced Ca^{2+} responses (Wicks et al., 2011). However, the differences in spectral sensitivity and G protein coupling of rhodopsin and of the UVR pathway suggest that rhodopsin might work in conjunction with a different, possibly unidentified, UVR-sensitive receptor to mediate UVR phototransduction in melanocytes. Future experiments will identify the UVR receptor and determine the molecular mechanism of TRPA1 activation. Understanding this pathway might uncover new photoprotection strategies for human skin, thus lowering the incidence of skin cancer.

We thank Dr. Sharona Gordon for generously providing the recombinant PH domains and Dr. Anita Zimmerman for helpful discussion.

This work was funded by grants from Brown University, NIH RI-INBRE 8P20GM103430-12, subaward No. 120912/0003223 (to E. Oancea), a National Science Foundation Graduate Research Fellowship (to N.W. Bellono), and National Institutes of Health Predoctoral Fellowship (NIAMS-NIH [F31] No. AR056587 to J.A. Najera).

The authors declare no competing financial interests.

Author contributions: J.A. Najera, N.W. Bellono, and E. Oancea designed the research in the paper; J.A. Najera and N.W. Bellono performed the research; E. Oancea contributed new reagents/analytic tools; J.A. Najera and N.W. Bellono analyzed data; and J.A. Najera, N.W. Bellono, and E. Oancea wrote the paper.

Edward N. Pugh Jr. served as editor.

Submitted: 23 August 2013
Accepted: 2 January 2014

REFERENCES

Bandell, M., G.M. Story, S.W. Hwang, V. Viswanath, S.R. Eid, M.J. Petrus, T.J. Earley, and A. Patapoutian. 2004. Noxious cold ion channel TRPA1 is activated by pungent compounds and bradykinin. *Neuron.* 41:849–857. http://dx.doi.org/10.1016/S0896-6273(04)00150-3

Barr, A.J., H. Ali, B. Haribabu, R. Snyderman, and A.V. Smrcka. 2000. Identification of a region at the N-terminus of phospholipase C-beta 3 that interacts with G protein beta gamma subunits. *Biochemistry.* 39:1800–1806. http://dx.doi.org/10.1021/bi992021f

Beckman, B., J. Flores, P.A. Witkum, and G.W. Sharp. 1974. Studies on the mode of action of cholera toxin. Effects on solubilized adenylate cyclase. *J. Clin. Invest.* 53:1202–1205. http://dx.doi.org/10.1172/JCI107660

Bellono, N.W., and E. Oancea. 2013. UV light phototransduction depolarizes human melanocytes. *Channels (Austin).* 7:243–248. http://dx.doi.org/10.4161/chan.25322

Bellono, N.W., L.G. Kammel, A.L. Zimmerman, and E. Oancea. 2013. UV light phototransduction activates transient receptor potential A1 ion channels in human melanocytes. *Proc. Natl. Acad. Sci. USA.* 110:2383–2388. http://dx.doi.org/10.1073/pnas.1215555110

Bennett, D.C. 2008. Ultraviolet wavebands and melanoma initiation. *Pigment Cell Melanoma Res.* 21:520–524. http://dx.doi.org/10.1111/j.1755-148X.2008.00500.x

Berson, D.M., F.A. Dunn, and M. Takao. 2002. Phototransduction by retinal ganglion cells that set the circadian clock. *Science.* 295:1070–1073. http://dx.doi.org/10.1126/science.1067262

Dai, Y., S. Wang, M. Tominaga, S. Yamamoto, T. Fukuoka, T. Higashi, K. Kobayashi, K. Obata, H. Yamanaka, and K. Noguchi. 2007. Sensitization of TRPA1 by PAR2 contributes to the sensation of inflammatory pain. *J. Clin. Invest.* 117:1979–1987. http://dx.doi.org/10.1172/JCI30951

De Vries, L., B. Zheng, T. Fischer, E. Elenko, and M.G. Farquhar. 2000. The regulator of G protein signaling family. *Annu. Rev. Pharmacol. Toxicol.* 40:235–271. http://dx.doi.org/10.1146/annurev.pharmtox.40.1.235

Fung, B.K., J.B. Hurley, and L. Stryer. 1981. Flow of information in the light-triggered cyclic nucleotide cascade of vision. *Proc. Natl. Acad. Sci. USA.* 78:152–156. http://dx.doi.org/10.1073/pnas.78.1.152

Gafni, J., J.A. Munsch, T.H. Lam, M.C. Catlin, L.G. Costa, T.F. Molinski, and I.N. Pessah. 1997. Xestospongins: potent membrane permeable blockers of the inositol 1,4,5-trisphosphate receptor.

Neuron. 19:723–733. http://dx.doi.org/10.1016/S0896-6273(00)80384-0

Goubaeva, F., M. Ghosh, S. Malik, J. Yang, P.M. Hinkle, K.K. Griendling, R.R. Neubig, and A.V. Smrcka. 2003. Stimulation of cellular signaling and G protein subunit dissociation by G protein betagamma subunit-binding peptides. *J. Biol. Chem.* 278:19634–19641. http://dx.doi.org/10.1074/jbc.M300052200

Graham, D.M., K.Y. Wong, P. Shapiro, C. Frederick, K. Pattabiraman, and D.M. Berson. 2008. Melanopsin ganglion cells use a membrane-associated rhabdomeric phototransduction cascade. *J. Neurophysiol.* 99:2522–2532. http://dx.doi.org/10.1152/jn.01066.2007

Hardie, R.C. 2001. Phototransduction in *Drosophila melanogaster. J. Exp. Biol.* 204:3403–3409.

Heximer, S.P. 2004. RGS2-mediated regulation of Gqalpha. *Methods Enzymol.* 390:65–82.

Heximer, S.P., N. Watson, M.E. Linder, K.J. Blumer, and J.R. Hepler. 1997. RGS2/G0S8 is a selective inhibitor of Gqalpha function. *Proc. Natl. Acad. Sci. USA.* 94:14389–14393. http://dx.doi.org/10.1073/pnas.94.26.14389

Imokawa, G., Y. Yada, and M. Miyagishi. 1992. Endothelins secreted from human keratinocytes are intrinsic mitogens for human melanocytes. *J. Biol. Chem.* 267:24675–24680.

Karashima, Y., J. Prenen, V. Meseguer, G. Owsianik, T. Voets, and B. Nilius. 2008. Modulation of the transient receptor potential channel TRPA1 by phosphatidylinositol 4,5-biphosphate manipulators. *Pflugers Arch.* 457:77–89. http://dx.doi.org/10.1007/s00424-008-0493-6

Kim, D., E.J. Cavanaugh, and D. Simkin. 2008. Inhibition of transient receptor potential A1 channel by phosphatidylinositol-4,5-bisphosphate. *Am. J. Physiol. Cell Physiol.* 295:C92–C99. http://dx.doi.org/10.1152/ajpcell.00023.2008

Klein, R.M., C.A. Ufret-Vincenty, L. Hua, and S.E. Gordon. 2008. Determinants of molecular specificity in phosphoinositide regulation. Phosphatidylinositol (4,5)-bisphosphate (PI(4,5)P2) is the endogenous lipid regulating TRPV1. *J. Biol. Chem.* 283:26208–26216. http://dx.doi.org/10.1074/jbc.M801912200

Lukacs, V., B. Thyagarajan, P. Varnai, A. Balla, T. Balla, and T. Rohacs. 2007. Dual regulation of TRPV1 by phosphoinositides. *J. Neurosci.* 27:7070–7080. http://dx.doi.org/10.1523/JNEUROSCI.1866-07.2007

Malbon, C.C., P.J. Rapiejko, and J.A. Garciá-Sáinz. 1984. Pertussis toxin catalyzes the ADP-ribosylation of two distinct peptides, 40 and 41 kDa, in rat fat cell membranes. *FEBS Lett.* 176:301–306. http://dx.doi.org/10.1016/0014-5793(84)81184-9

Malik, S., M. Ghosh, T.M. Bonacci, G.G. Tall, and A.V. Smrcka. 2005. Ric-8 enhances G protein betagamma-dependent signaling in response to betagamma-binding peptides in intact cells. *Mol. Pharmacol.* 68:129–136.

Mukai, H., E. Munekata, and T. Higashijima. 1992. G protein antagonists. A novel hydrophobic peptide competes with receptor for G protein binding. *J. Biol. Chem.* 267:16237–16243.

Oancea, E., M.N. Teruel, A.F. Quest, and T. Meyer. 1998. Green fluorescent protein (GFP)-tagged cysteine-rich domains from protein kinase C as fluorescent indicators for diacylglycerol signaling in living cells. *J. Cell Biol.* 140:485–498. http://dx.doi.org/10.1083/jcb.140.3.485

Oka, T., K. Sato, M. Hori, H. Ozaki, and H. Karaki. 2002. Xestospongin C, a novel blocker of IP3 receptor, attenuates the increase in cytosolic calcium level and degranulation that is induced by antigen in RBL-2H3 mast cells. *Br. J. Pharmacol.* 135:1959–1966. http://dx.doi.org/10.1038/sj.bjp.0704662

Panda, S., S.K. Nayak, B. Campo, J.R. Walker, J.B. Hogenesch, and T. Jegla. 2005. Illumination of the melanopsin signaling pathway. *Science.* 307:600–604. http://dx.doi.org/10.1126/science.1105121

Park, D., D.Y. Jhon, C.W. Lee, K.H. Lee, and S.G. Rhee. 1993. Activation of phospholipase C isozymes by G protein beta gamma subunits. *J. Biol. Chem.* 268:4573–4576.

Park, H.Y., M. Kosmadaki, M. Yaar, and B.A. Gilchrest. 2009. Cellular mechanisms regulating human melanogenesis. *Cell. Mol. Life Sci.* 66:1493–1506. http://dx.doi.org/10.1007/s00018-009-8703-8

Routaboul, C., A. Denis, and A. Vinche. 1999. Immediate pigment darkening: description, kinetic and biological function. *Eur. J. Dermatol.* 9:95–99.

Roy, A.A., A. Baragli, L.S. Bernstein, J.R. Hepler, T.E. Hébert, and P. Chidiac. 2006. RGS2 interacts with Gs and adenylyl cyclase in living cells. *Cell. Signal.* 18:336–348. http://dx.doi.org/10.1016/j.cellsig.2005.05.004

Smrcka, A.V., J.R. Hepler, K.O. Brown, and P.C. Sternweis. 1991. Regulation of polyphosphoinositide-specific phospholipase C activity by purified Gq. *Science.* 251:804–807. http://dx.doi.org/10.1126/science.1846707

Suh, B.C., and B. Hille. 2005. Regulation of ion channels by phosphatidylinositol 4,5-bisphosphate. *Curr. Opin. Neurobiol.* 15:370–378. http://dx.doi.org/10.1016/j.conb.2005.05.005

Taylor, S.J., H.Z. Chae, S.G. Rhee, and J.H. Exton. 1991. Activation of the beta 1 isozyme of phospholipase C by alpha subunits of the Gq class of G proteins. *Nature.* 350:516–518. http://dx.doi.org/10.1038/350516a0

Ufret-Vincenty, C.A., R.M. Klein, L. Hua, J. Angueyra, and S.E. Gordon. 2011. Localization of the PIP2 sensor of TRPV1 ion channels. *J. Biol. Chem.* 286:9688–9698. http://dx.doi.org/10.1074/jbc.M110.192526

Wang, Y.F., and G.I. Hatton. 2007. Dominant role of betagamma subunits of G-proteins in oxytocin-evoked burst firing. *J. Neurosci.* 27:1902–1912. http://dx.doi.org/10.1523/JNEUROSCI.5346-06.2007

Wang, S., Y. Dai, T. Fukuoka, H. Yamanaka, K. Kobayashi, K. Obata, X. Cui, M. Tominaga, and K. Noguchi. 2008. Phospholipase C and protein kinase A mediate bradykinin sensitization of TRPA1: a molecular mechanism of inflammatory pain. *Brain.* 131:1241–1251. http://dx.doi.org/10.1093/brain/awn060

Wicks, N.L., J.W. Chan, J.A. Najera, J.M. Ciriello, and E. Oancea. 2011. UVA phototransduction drives early melanin synthesis in human melanocytes. *Curr. Biol.* 21:1906–1911. http://dx.doi.org/10.1016/j.cub.2011.09.047

Wilson, S.R., K.A. Gerhold, A. Bifolck-Fisher, Q. Liu, K.N. Patel, X. Dong, and D.M. Bautista. 2011. TRPA1 is required for histamine-independent, Mas-related G protein-coupled receptor-mediated itch. *Nat. Neurosci.* 14:595–602. http://dx.doi.org/10.1038/nn.2789

Wu, D., A. Katz, and M.I. Simon. 1993. Activation of phospholipase C beta 2 by the alpha and beta gamma subunits of trimeric GTP-binding protein. *Proc. Natl. Acad. Sci. USA.* 90:5297–5301. http://dx.doi.org/10.1073/pnas.90.11.5297

Xiang, Y., Q. Yuan, N. Vogt, L.L. Looger, L.Y. Jan, and Y.N. Jan. 2010. Light-avoidance-mediating photoreceptors tile the *Drosophila* larval body wall. *Nature.* 468:921–926. http://dx.doi.org/10.1038/nature09576

Yada, Y., K. Higuchi, and G. Imokawa. 1991. Effects of endothelins on signal transduction and proliferation in human melanocytes. *J. Biol. Chem.* 266:18352–18357.

Yau, K.W., and R.C. Hardie. 2009. Phototransduction motifs and variations. *Cell.* 139:246–264. http://dx.doi.org/10.1016/j.cell.2009.09.029